Geomechanics for Energy and the Environment 4 (2015) 51–60

Contents lists available at ScienceDirect

Geomechanics for Energy and the Environment

journal homepage: www.elsevier.com/locate/gete

A hydromechanical approach to assess CO_2 injection-induced surface uplift and caprock deflection

Chao Li *, Paul Barès, Lyesse Laloui

Laboratory of Soil Mechanics - Chair "Gaz Naturel" Petrosvibri, Swiss Federal Institute of Technology, EPFL, Lausanne, Switzerland

HIGHLIGHTS

- A semi-analytical solution is proposed to assess CO_2 injection in deformable medium.
- Good agreement is found between the proposed solution and the finite element method.
- Geomechanical interactions between a caprock and adjacent regions are examined.
- The surface uplift measured at In Salah can be reproduced by the proposed solution.

ARTICLE INFO

Article history:
Received 16 June 2015
Accepted 23 June 2015
Available online 4 July 2015

Keywords:
CO_2 injection
Semi-analytical coupled solution
Surface uplift
Caprock deformation
In Salah project

ABSTRACT

This study focuses on the derivation of a semi-analytical approach for the evaluation of surface uplift and caprock deflection induced by underground injection of CO_2. The adopted methodology includes the development of a mathematical model that incorporates the deformable behaviour of the storage reservoir and the flow of two immiscible fluids (CO_2 and brine) within the aquifer while the surface rock or the caprock layer is modelled as a thin plate. Governing equations are solved for the axisymmetric flexural deflection due to a constant rate of CO_2 injection. Both developed solutions are applied to a representative CO_2 storage case solved numerically by the finite element method, and good agreement between results is observed. When benchmarking to the In Salah surface uplift, the developed semi-analytical approach can capture a high rate of surface uplift caused by the pressure build-up during the early stage of CO_2 injection. The required calculation time is very short compared to a classical finite element approach. This method can be employed as a design tool for the analysis of uncertainty in parameters such as the injection rate, porosity, rock properties and geological structures. This semi-analytical approach also provides an efficient means of estimating the influence of high injection rates of CO_2 on surface uplift.

1. Introduction

The combustion of oil, natural gas and coal accounts for approximately 80% of the world's energy and releases approximately 30 billion tonnes of carbon dioxide (CO_2) per year into the atmosphere.[1] The increased emission of CO_2 and resulting greenhouse effect have been implicated in global warming.[2] Geological sequestration of CO_2 is a technology to mitigate the amount of carbon dioxide, in accordance with the Kyoto Protocol, entering the atmosphere by capturing and storing the CO_2 from industrial emissions. This technology thus enables the continued use of fossil fuels. Deep saline aquifers are considered the most suitable geological formations for CO_2 storage because of their large capacity to trap CO_2.[3]

High rate (>1 Mt/year) injection of CO_2 into an aquifer results in an abrupt fluid pressure build-up, disturbing the stress state and generating deformations within the injection area. These hydromechanical variations spread both

* Correspondence to: Laboratory of Soil Mechanics - Chair "Gaz Naturel" Petrosvibri, EPFL-ENAC-IIC-LMS, Station 18, CH-1015 Lausanne, Switzerland.
E-mail address: chao.li@epfl.ch (C. Li).

http://dx.doi.org/10.1016/j.gete.2015.06.002
2352-3808/

Nomenclature

J_n	Bessel function of the first kind of order n
l	Distance from the caprock to the middle of the injection zone
m	Aquifer (injection zone) thickness
h	Caprock thickness
w	Deflection
α_s	Biot's coefficient
G_s	Storage unit shear modulus
G_c	Caprock shear modulus
G_o	Overburden unit shear modulus
ν_s	Storage unit Poisson's ratio
ν_c	Caprock Poisson's ratio
ν_o	Overburden unit Poisson's ratio
Ω	Material property constant of the medium
Φ	Material property constant of the medium
g	Gravity
k	Intrinsic permeability
$\overline{\Delta p}$	Fluid overpressure density after the Hankel transformation
Q_m	CO_2 mass flow rate
Q_0	CO_2 volumetric flow rate
R	Radius of influence
r	Radial distance
r_0	CO_2 plume radius at the top of the aquifer
r_b	CO_2 plume radius at the base of the aquifer
r_w	Injection well radius
S_s	Specific storage coefficient (Bear[20])
t	Time
T	Temperature
z	Vertical coordinate
$V(t)$	CO_2 plume volume $V(t) = Q_0 t$
α	Phase index, $c = CO_2$ and $w =$ brine
μ_α	Viscosity of α-phase ($\alpha = c, w$)
ρ_c	Mean CO_2 density
ρ_w	Water density
ϕ	Porosity
ζ	Interface position from the bottom of the aquifer
NB	Nordbotten et al.[16] approach
DZ	Dentz and Tartakovsky[17] approach
LI–SN	Developed Li–Selvadurai–Nordbotten solution
LI–SD	Developed Li–Selvadurai–Dentz solution

laterally and vertically. Induced deformation may propagate to the surface[4] and cause surface uplift. Ground deformation of up to 7 mm/year has been measured around each of the three injection wells at the In Salah project, Algeria, the largest on-shore CO_2 storage project in the world.[5,6] These geomechanical issues have become a public concern and a research and industry interest for future reservoir integrity design and risk assessment of CO_2 storage projects.

Relying on representative geometries, many studies use computational approaches (finite difference, finite volume and finite element) to study this hydromechanical coupled behaviour.[7–10] Although these approaches can address the problem, significant efforts and costs are required to construct numerical models for each potential candidate site and for uncertainty studies of geometric, geological and material parameters. Analytical solutions or semi-analytical approaches may be more suitable because of their computational efficiency and ability to identify driving mechanisms. Due to the complexity of the hydromechanical coupling effects and multiphase fluid interactions induced by CO_2 injection, current analytical and semi-analytical approaches may lose their forecasting capacity and reliability for the geomechanical analysis of CO_2 injection due to certain model assumptions, as described below.

Rutqvist[11] estimated the surface uplift at In Salah using a simplified analytical solution according to Fjar.[12] The estimate is within the correct order of magnitude but has an overestimation of more than 50%. Various assumptions restrict the applicability of this solution, such as the consideration of a unique layered reservoir, 1-dimensional geometry and a uniformly distributed and constant injection-induced overpressure. Other advanced semi-analytical approaches can consider more complex geometries and additional mechanical mechanisms, such as multi-layered reservoirs and the effect of the bending moment between layers.[13–15] Nevertheless, these solutions only consider a flat, constant and fixed pressure as a loading variable. The injection-induced effects on the temporal and spatial evolution of the overpressure and of the reservoir deformation are thus omitted.

To provide a contribution to the pioneer works of Selvadurai[14,15] and Rutqvist,[11] we propose a novel semi-analytical approach to overcome the former limitations. Based on a representative geometry for CO_2 storage, the proposed approach assesses the spatial and temporal surface uplift and caprock deformation caused by CO_2 pressurization and evaluates critical parameters for project design and risk management, including injection rate, permeability of the aquifer, thickness of the caprock, location of the injection zone and mechanical properties of the reservoir. We first derive a mathematical model to calculate the caprock and surface deformation caused by an arbitrary pressurization within the injection zone; this model extends the embedded plate approach proposed by Selvadurai.[14,15] This is followed by the incorporation of injection-induced overpressure distribution functions originating from two analytical solutions proposed by Nordbotten et al.[16] and Dentz and Tartakovsky.[17] After mathematical integration, the analytical modelling produces two semi-analytical solutions that can address CO_2 injection-induced effects on the geomechanical behaviour of the reservoir. Such solutions have not been derived previously. A comparison with a finite element approach is then proposed to evaluate the performance of the semi-analytical solutions, followed by a parametric study to illustrate how such solutions can be applied to examine the effects of the geometric and physical parameters on caprock deformation. Finally, the developed solutions are benchmarked to the surface uplift problem at In Salah.

2. Caprock deformation due to pressurization

2.1. Model description

As shown in Fig. 1, an axisymmetric system is proposed for a typical CO_2 storage problem. The system consists of

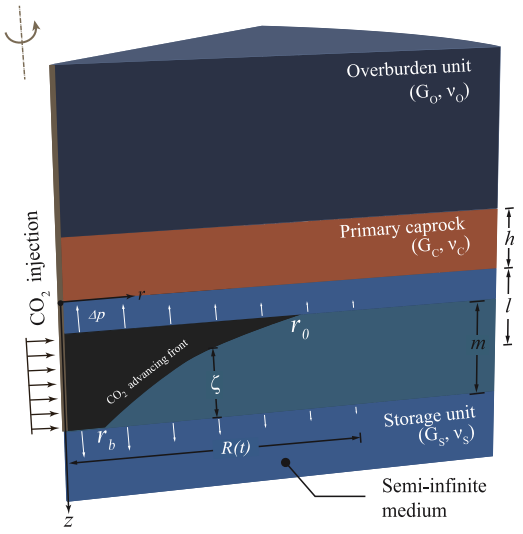

Fig. 1. Idealized configuration of an embedded caprock layer.

an overburden region and a saturated storage unit with a primary caprock embedded in between. CO_2 is injected into an m-metre-thick target aquifer with a distance l to the primary caprock layer of h metres thick. The injection zone is confined by impermeable strata. Injection of CO_2 through a vertical injection well causes pressurization within the injection zone, resulting in caprock deformation. The pressurization vanishes in the direction radial to the position with radius of influence R, at which the pressure equals the initial hydrostatic pressure. This radius of influence extends in the radial direction as injection continues and is therefore time-dependent. For caprock deformation, Selvadurai[14,15] proposed an elastic solution in which the caprock is modelled as an embedded plate over a circular region of flat and constant pressurization. Based on his approach, we focus on the extension of the model to account for arbitrary pressurization distributions. The corresponding caprock deflection is derived under this pressure loading.

2.2. Embedded plate approach

Selvadurai[14,15] considered the caprock layer a thin plate embedded between the overburden region and the storage region. The overburden and storage regions are modelled as half-space regions. The assumption of a thin plate is justified by its thickness in relation to the dimensions (radius) of the pressurized zone. The interaction among the three units is caused by pressurization of a constant magnitude Δp applied over the entire injection zone.

The embedded caprock layer exhibits flexural behaviour that is governed by Germain–Poisson–Kirchhoff thin plate theory.[18] The governing equation employs polar coordinates with the Laplace operator $\tilde{\nabla}^2 = \frac{d^2}{dr^2} + \frac{1}{r}\frac{d}{dr}$:

$$D\tilde{\nabla}^2\tilde{\nabla}^2 w\,(r) + q^{(s)}\,(r) - q^{(o)}\,(r) = 0 \tag{1}$$

where the deflection $w\,(r)$ is constrained by contact stresses $q^{(s)}\,(r)$ and $q^{(o)}\,(r)$, which are applied on the contact faces between the caprock and the respective regions. The flexural rigidity of the embedded caprock layer is expressed by $D\left(=G_c h^3/6\,(1-\nu_c)\right)$ with thickness h of the caprock layer, shear modulus G_c and Poisson's ratio of the caprock ν_c. The pressurization of intensity Δp (Pa/m^3) is within the injection zone with a radius of influence R and thickness m located at a distance l from the interface between the caprock and the storage region. The caprock layer is assumed to be in bonded contact with the storage and overburden regions, for which the relevant kinematic interface conditions are as follows:

$$w\,(r, z=0) = u_z^{(s)q}\,(r,0) + u_z^{(s)p}\,(r,0) = u_z^{(o)q}\,(r,0) \tag{2}$$

$$u_r^{(s)}\,(r, z=0) = u_r^{(s)p}\,(r,0) = u_r^{(o)}\,(r,0) = 0 \tag{3}$$

where u_r and u_z are, respectively, the radial and axial displacement vector in the polar coordinates, u^p is the displacement due to overpressure Δp, and u^q is the displacement constrained by contact stress q.

2.3. Extension to arbitrary pressurization-induced deflection

We consider overpressure Δp not constant but time and space dependent. The caprock displacement due to an overpressure generation Δp of any form of distribution within the injection zone can be written with the aid of Green's function[19]:

$$u_z^{(s)p}\,(r,0) = \frac{\alpha_s}{G_s}\int_0^\infty\int_0^\infty \Delta p\,(\rho) \cdot g_z\,(r, z=0;\,\rho, d)\,\mathrm{d}\rho\mathrm{d}d \tag{4}$$

where

$$g_z\,(r, z=0;\,\rho, d) = -(1-2\nu_s)\,\rho\int_0^\infty \xi J_0(\xi r) J_0(\xi\rho) e^{-\xi d}\mathrm{d}\xi \tag{5}$$

is Green's function, which corresponds to a ring of dilatation at radius $\rho \in [0,\infty]$ and depth $d \in \left[l - m/2,\, l + m/2\right]$.

A necessary approximation for evaluating the integral is given by:

$$\int_{l-m/2}^{l+m/2} e^{-kd}\mathrm{d}d \approx m e^{-kl}. \tag{6}$$

This approximation has been stated in Geertsma[13] and Segall et al.[19] and is valid for the case in which the thickness of aquifer m is very small compared to its depth l to the caprock, for instance, in the application of surface subsidence due to depletion of a deep reservoir. Consequently, the assumption constrains the range of applications and is therefore not appropriate for the case in which the aquifer is situated just below or close to the caprock ($l = m/2$), a typical case for CO_2 storage that is one of the objectives of this study. This assumption has not been addressed since its first appearance in Geertsma[13] and it is necessary for deriving the next step of the mathematical formulation, but its restriction must be lifted. We demonstrate in Appendix A that the influence of the relationship between l and m on Green's function is not significant due to the decaying behaviour of the multiplication of two Bessel

functions in Eq. (5). In conclusion, the consequence of this assumption on the physical interpretation can be neglected, and its benefit to the mathematical derivation still holds.

To introduce a pressure distribution, the integral of Eq. (4) is expressed as follows:

$$u_z^{(s)p}(r,0) = -\frac{(1-2\nu_s)\,\alpha_s m}{G_s}\int_0^\infty \xi J_0(\xi r)e^{-\xi l} \times \int_0^\infty \rho\Delta p(\rho) J_0(\xi\rho)\mathrm{d}\rho\,\mathrm{d}\xi. \quad (7)$$

Eq. (7) shows a linear relationship between the displacement and the material properties (i.e., $1/G_s$ and ν_s). The displacement induced by pressurization depends on the Bessel integral of the overpressure distribution $\Delta p(\rho)$. Evaluating $u_z^{(s)p}(r,0)$ with the zeroth-order Hankel transform gives the following:

$$\bar{u}_z^{(s)p}(\xi) = -\frac{(1-2\nu_s)\,\alpha_s m}{G_s}\overline{\Delta p}(\xi)\,e^{-\xi l} \quad (8)$$

where $\overline{\Delta p}$ is the zeroth-order Hankel transform of Δp. This term yields the coupling term between pressurization and mechanical deflection.

Selvadurai[15] stated that the displacement was constrained by the contact stresses:

$$\bar{u}_z^{(s)q}(r,0) = \frac{(3-4\nu_s)}{4G_s(1-\nu_s)}\frac{1}{\xi}\bar{q}^s(\xi) \quad (9)$$

$$\bar{u}_z^{(o)q}(r,0) = \frac{(3-4\nu_o)}{4G_o(1-\nu_o)}\frac{1}{\xi}\bar{q}^o(\xi). \quad (10)$$

Combining the kinematic constraint to which the storage region is subjected (Eq. (2)), the displacement induced by the pressurization (Eq. (8)) and the restricted deflection by the contact stress (Eq. (9)), we obtain the following equation after the zeroth-order Hankel transform:

$$\bar{q}^s(\xi) = \frac{4G_s(1-\nu_s)}{(3-4\nu_s)}\xi\bar{w}(\xi) + \frac{4(1-\nu_s)(1-2\nu)\,\alpha_s m}{(3-4\nu_s)}\xi\overline{\Delta p}(\xi)\,e^{-\xi l}. \quad (11)$$

Considering the kinematic constraints Eqs. (2) and (10) on the storage region, we can obtain the following:

$$\bar{q}^o(\xi) = -\frac{4G_o(1-\nu_o)}{(3-4\nu_o)}\xi\bar{w}(\xi). \quad (12)$$

By evaluating the differential equation (1) with the zeroth-order Hankel transform:

$$D\xi^4\bar{w}(\xi) + \bar{q}^s(\xi) - \bar{q}^o(\xi) = 0 \quad (13)$$

and introducing Eqs. (11) and (12), we find the deflection of the caprock layer induced by an arbitrary radial pressurization after the inverse Hankel transformation:

$$w(r) = \frac{\Omega m}{h^2}\int_0^\infty \frac{\xi}{1+\Phi\xi^3}\overline{\Delta p}\left(\frac{\xi}{h}\right)e^{-\frac{\xi l}{h}}J_0\left(\frac{\xi r}{h}\right)\mathrm{d}\xi \quad (14)$$

where Ω and Φ are constants that depend on the properties of the medium:

$$\Omega = \frac{\alpha_s(1-\nu_s)(1-2\nu_s)(3-4\nu_o)}{G_s(1-\nu_s)(3-4\nu_o)+G_o(1-\nu_o)(3-4\nu_s)} \quad (15)$$

$$\Phi = \frac{(3-4\nu_s)(3-4\nu_o)G_c}{24(1-\nu_c)\left[G_s(1-\nu_s)(3-4\nu_o)+G_o(1-\nu_o)(3-4\nu_s)\right]}. \quad (16)$$

Eq. (14) extends the solution of Selvadurai[14,15] to the case of a non-uniform distribution of overpressure and uses the Hankel transformation $\overline{\Delta p}$ to introduce any continuous overpressure evolution functions.

3. Caprock deflection induced by CO_2 injection

To determine the deflection $w(r)$ according to Eq. (14), the overpressure distribution $\overline{\Delta p}$ must be allocated to describe the distribution of centres of pressurization. Selvadurai[14,15] considers a constant overpressure distributed within the injection zone. However, CO_2 injection results in a high concentration of overpressure around the injection well, and this overpressure vanishes with distance. This overpressure pattern is necessary to estimate the magnitude of the deformation more accurately and can be derived from two analytical solutions proposed by Nordbotten et al.[16] and Dentz and Tartakovsky,[17] which describe the advancing abrupt interface between the injected CO_2 and the host water, which are assumed to be immiscible. As shown in Fig. 1, the injection zone is divided into three regions: (1) around the injection well, where only injected CO_2 exists ($r \le r_b$); (2) the intermediate region, where the two fluids coexist but are separated by a sharp interface ($r_b \le r \le r_0$); and (3) the outer region, where only host water exists ($r_0 \le r \le R$). The governing equation for the interface position is derived by Bear[20]:

$$\frac{1}{r}\frac{\partial}{\partial r}\left[\zeta\frac{Q_0 - 2\pi r(\rho_w-\rho_c)g(k/\mu_c)(m-\zeta)\,\partial\zeta/\partial r}{\zeta+(m-\zeta)\,\mu_w/\mu_c}\right] + 2\pi\phi\frac{\partial\zeta}{\partial t} = 0, \quad (17)$$

where Q_0 is the volumetric flux rate of injected CO_2 and ζ denotes the vertical position of the interface between the two fluids. Both solutions (Nordbotten et al.[16] and Dentz and Tartakovsky[17]) are approximations of the exact solution of Eq. (17) but differ in the assumptions made for the approximation. Whereas Nordbotten et al.[16] used an energy minimization approximation, Dentz and Tartakovsky[17] applied the Dupuit assumption of horizontal flow. The development of the solutions is not detailed in this paper; the reader is referred to the original works of Nordbotten et al.[16] and Dentz and Tartakovsky.[17] In addition, the validity and the applicability of both solutions has been discussed in.[21–23]

The interface solutions derived by Nordbotten et al.,[16] denoted by NB, and Dentz and Tartakovsky,[17] denoted by DZ, are written as follows:

$$\zeta_{NB}(r,t) = m\left[1-\frac{\mu_c}{\mu_w-\mu_c}\left(\sqrt{\frac{\mu_w Q_0 t}{\mu_c\phi\pi mr^2}}-1\right)\right] \quad (18)$$

$$\zeta_{DZ}(r,t) = \frac{Q_0}{2\pi kmg}\frac{\mu_w-\mu_c}{\rho_w-\rho_c}\ln\left(\frac{r}{r_{b,DZ}(t)}\right) \quad (19)$$

where $r_b(t)$ is the radius at which the interface intersects the lower domain boundary and is determined by the volume conservation (Dentz and Tartakovsky[17]):

$$r_{b,DZ}(t) = 2\sqrt{\frac{tkmg(\rho_w-\rho_c)}{\phi(\mu_w-\mu_c)}\left[\exp\left(\frac{4\pi km^2 g(\rho_w-\rho_c)}{Q_0(\mu_w-\mu_c)}\right)-1\right]^{-1}}. \quad (20)$$

We further account for the pressure-dependent CO_2 density and viscosity according to Peng and Robinson[24] and Fenghour et al.,[25] respectively, through the iterative methodology proposed by Vilarrasa et al.[23] Inserting interface Eqs. (18) and (19) into the integration of Darcy's law results in the derivation of two vertically averaged overpressure expressions with the zeroth-order Hankel transformation. The transformed expressions are substituted into the mechanical deflection Eq. (14), which leads to two hydromechanical solutions, the Li–Selvadurai–Nordbotten solution, denoted by LI–SN, and the Li–Selvadurai–Dentz solution, denoted by LI–SD, as shown below. These solutions permit the analysis of the interaction between the caprock and surrounding regions that are subjected to CO_2 injection-induced pressurization.

$$\begin{aligned} w(r)_{LI-SN} = {} & \frac{\Omega m}{h^2}\int_0^\infty \frac{\xi e^{-\frac{\xi l}{h}}}{1+\Phi\xi^3} \\ & \times\left\{\frac{Ah^2}{\xi^2}\left[y\ln\left(\frac{yh}{\xi R}\right)J_1(y)+J_0(y)\right]_{\xi R/h}^{\xi r_0/h}\right. \\ & +A\left(\ln\left(\frac{R}{r_0}\right)+Br_0\right) \\ & \times\frac{r_0J_1(\xi r_0/h)-r_bJ_1(\xi r_b/h)}{\xi/h} \\ & -AB\int_{r_b}^{r_0} r^2J_0(\xi r/h)\mathrm{d}r+\frac{ACh^2}{\xi^2} \\ & \times\left[y\ln\left(\frac{yh}{\xi r_b}\right)J_1(y)+J_0(y)\right]_{\xi r_b/h}^{\xi r_w/h} \\ & +A\left(\ln\left(\frac{R}{r_0}\right)+B(r_0-r_b)\right) \\ & \left.\times\frac{r_bJ_1(\xi r_b/h)-r_wJ_1(\xi r_w/h)}{\xi/h}\right\} \\ & \times J_0\left(\frac{\xi r}{h}\right)\mathrm{d}\xi \end{aligned} \quad (21)$$

with parameters $A=\frac{Q_0\mu_w}{2\pi km}$; $B=\sqrt{\frac{\mu_c\phi\pi m}{\mu_w V(t)}}$; $C=\frac{\mu_c}{\mu_w}$ and $R=\sqrt{\frac{2.25k\rho_w gt}{\mu_w S_s}}$.

$$\begin{aligned} w(r)_{LI-SD} = {} & \frac{\Omega m}{h^2}\int_0^\infty \frac{\xi e^{-\frac{\xi l}{h}}A}{(1+\Phi\xi^3)\mu_w} \\ & \times\left\{\frac{\mu_w h^2}{\xi^2}\left[y\ln\left(\frac{yh}{\xi R}\right)J_1(y)+J_0(y)\right]_{\xi R/h}^{\xi r_0/h}\right. \\ & +\hat{B}\frac{r_0J_1(\xi r_0/h)-r_wJ_1(\xi r_w/h)}{\xi/h} \\ & +\frac{\mu_c h^2}{\xi^2}\left[y\ln\left(\frac{yh}{r_b\xi}\right)J_1(y)+J_0(y)\right]_{\xi r_0/h}^{\xi r_w/h} \\ & \left.+\hat{C}\int_{r_b}^{r_0} r\ln\left(\frac{r}{r_b}\right)\ln\left(\frac{r_b}{r}\right)J_0\left(\frac{\xi r}{h}\right)\mathrm{d}r\right\} \\ & \times J_0\left(\frac{\xi r}{h}\right)\mathrm{d}\xi \end{aligned} \quad (22)$$

and parameters $\hat{B}=\mu_w\ln\left(\frac{R}{r_b}\right)-\frac{\mu_w-\mu_c}{2\gamma}$; $\hat{C}=\frac{(\mu_w-\mu_c)\gamma}{2}$ where $\gamma=\frac{Q_0(\mu_w-\mu_c)}{2\pi km^2g(\rho_w-\rho_c)}$.

4. Model verification

The two semi-analytical solutions Eqs. (21) and (22) are applied to a CO_2 storage injection problem to evaluate their performance in comparison with a numerical solution. The semi-analytical modelling described above assumes an elastic plate-like caprock and two immiscible fluids separated by an abrupt interface, whereas the numerical model considers poroelasticity and two miscible fluids with a capillary effect (detailed in Appendix B). The intent of the developed semi-analytical approach is to provide a straightforward and efficient tool for examining material sensitivity and geometric uncertainty. However, comparing the semi-analytical and numerical approaches can facilitate the assessment of the relevancy of our approximations.

A typical CO_2 storage model in an axisymmetric configuration is proposed, and the mesh for the numerical model is shown in Fig. B.1 of Appendix B. CO_2 is injected into a 100-m-thick aquifer at 100 kg/s through a vertical well of radius $r_w = 0.15$ m. The aquifer is situated 900 m underground and is overlaid by a 100-m-thick impermeable caprock. To approach the infinite-acting aquifer of the analytical solution, the numerical model is set at 10 km, and hydrostatic pressure and fixed displacement are applied on the outer boundary. The mechanical and hydraulic properties are given in Table 1. The nonlinear finite element FEM code Lagamine[27] is used to solve the problem numerically, and Matlab® is employed to compute the infinite integration of the two semi-analytical solutions.

The analytical versus numerical results are presented in Figs. 2 and 3 for the overpressure and caprock deflection distribution, respectively. The numerical results exhibit a slightly higher overpressure generation near the well field. This higher overpressure generation can be explained by the neglect of the capillary effect in semi-analytical approaches, which lowers the energy needed for CO_2 injection into the saturated aquifer. Furthermore, the numerical model describes a lower caprock deflection around the well. Because the coupling effect is relatively strong around the well, the poroelasticity theory in the numerical model allows more energy dissipation than the embedded plate approach in the semi-analytical method. Differences in the curvature of the deflection shape are also observed because the overpressure decreases logarithmically with distance in the LI–SD solution but linearly in the LI–SN solution and in numerical approach. However, the differences remain subtle. Both the overpressure and deflection calculated by the numerical approach are, on average, in good agreement with the analytical results.

Table 1
Parameter values used in the numerical experiments.

Analytical model	Symbol	Unit	Overburden unit	Storage unit	Caprock layer
Shear modulus	Go, Gs, Gc	GPa	1	10	5
Poisson's ratio	ν_o, ν_s, ν_c	–	0.25	0.25	0.25
Porosity in the injection zone	ϕ	–		0.15	–
Permeability in the injection zone	k	m^2		1.0e−13	–
Thickness of the caprock	m	m	100		
Distance from the caprock to the middle of the injection zone	l	m	50		
Well radius	r_w	m	0.15		
Injection rate	Q_m	kg/s	100		
Numerical model	**Retention curve**		**Relative permeability**		
van Genuchten[a]	$S_w = \left(1 + (s/P_0)^{1/(1-\lambda)}\right)^{-\lambda}$ $P_0 = 0.02$ MPa and $\lambda = 0.8$		$k_\alpha = S_\alpha$ $\alpha = CO_2; water$		
CO_2 density			Peng and Robinson[24]		
CO_2 viscosity			Fenghour et al.[25]		

[a] Linear relative permeabilities and a van Genuchten retention curve[26] parameter are set to approximate the abrupt interface approach.[23]

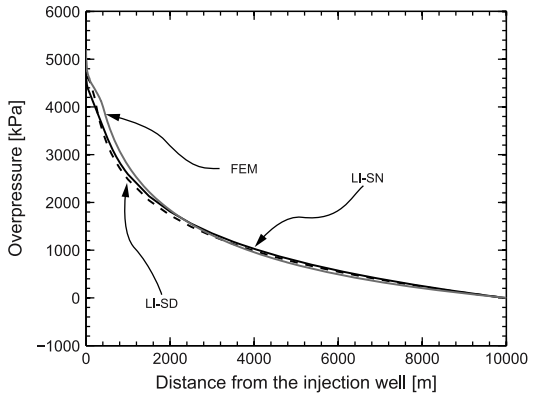

Fig. 2. Spatial distribution of the vertically averaged overpressure after 100 days of injection with the reference parameters.

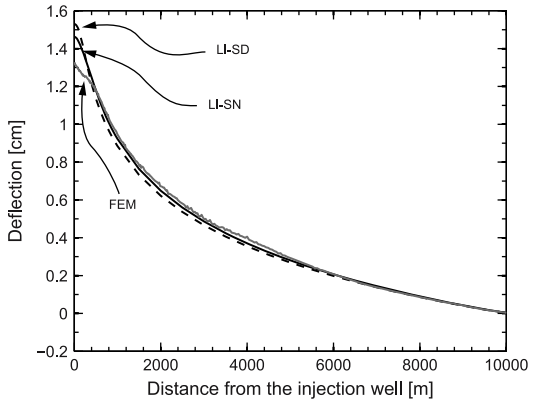

Fig. 3. Spatial distribution of the deflection of the caprock after 100 days of injection with the reference parameters.

5. Parametric studies

Based on the CO_2 storage problem described above, the effects of the geometric and the material parameters on the caprock deflection are studied. Fig. 4 shows the relationship between the deflection of the caprock and the distance to the injection zone. The magnitude of the

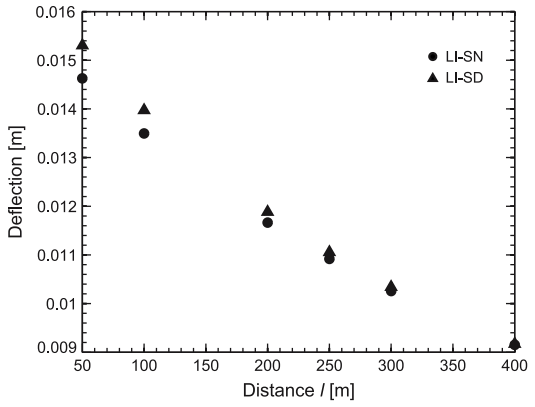

Fig. 4. Maximum deflection calculated after 100 days of injection at different distances l from the interface between the caprock and the aquifer.

overpressure decreases when the distance l is increased. The CO_2 density increases as the hydrostatic pressure increases with depth; thus, for a given mass of injected CO_2, the injected volume decreases and less overpressure accumulates. Because the estimated overpressure at the injection well is higher when using the LI–SD solution compared to the LI–SN solution, a higher overpressure is obtained with the LI–SD solution with a nearly constant difference in magnitude. The thickness of the zone between the caprock and the injection zone limits strain propagation from the injection zone to the caprock. Hence, the difference in the magnitude of deflection at the caprock vanishes with distance l, whereas the difference in the overpressure remains nearly constant (see Fig. 5). The effect of the overpressure difference is most significant when both layers are adjacent and becomes negligible when $l = 400$ m, suggesting that injection of CO_2 at a certain distance from the primary caprock can reduce the strain within the caprock and further reduce the possibility of fissuring and cracking.

The temporal evolution of the caprock deflection is shown in Fig. 6 with various permeabilities. At a constant rate of injection, the fluid pressure increases significantly at the beginning of the injection period. As a consequence

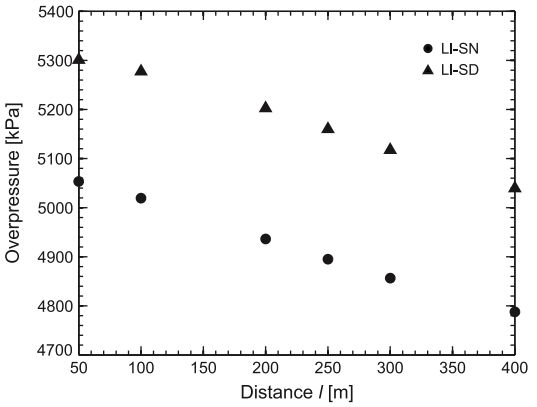

Fig. 5. Vertically averaged overpressure at the injection well after 100 days of injection at different distances l from the interface between the caprock and the aquifer.

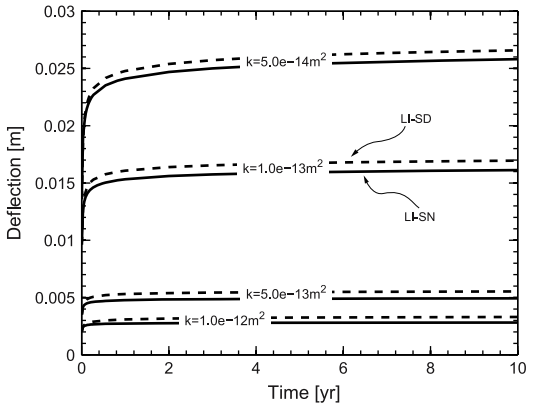

Fig. 6. Deflection at the injection well with time with variation in permeability.

of the elastic model, the deflection reflects the effect of overpressure and exhibits the same behaviour. The deflection increases gradually after one year of injection and reaches a maximum. The deflection is nearly proportional to the inverse of the permeability (see Eqs. (21) and (22)). Thus, the permeability can be considered an important factor to limit overpressure accumulation and subsequent deflection.

6. Benchmark to the case of the in Salah project

At In Salah, ground deformation was detected around three CO_2 injection wells by satellite imaging.[5,6,28] Because highly accurate measurements are available, the surface heave at In Salah is considered an ideal benchmark problem for geomechanical modelling. Using these data, Rutqvist et al.[8] and Preisig and Prévost[7] investigated the surface uplift around injection well KB501 using 3D and 2D numerical models, respectively. The results are in good agreement with the field measurements. Here, we apply our semi-analytical solutions to the same data set used by Rutqvist et al.[8] to assess the same problem. Instead of a three-dimensional analysis, we perform our analytical

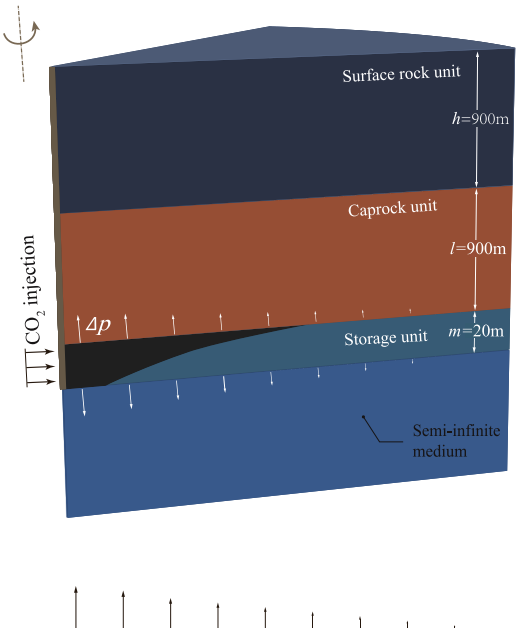

Fig. 7. Geometry of the model used to simulate the surface uplift around injection well KB501 at In Salah.

Table 2
Material parameters used in the simulation of the In Salah uplift.

Parameter	Unit	Caprock	Surface layer
Shear modulus	GPa	8.35	0.625
Poisson's ratio	–	0.2	0.2
Porosity in the injection zone	–	0.17	
Permeability in the injection zone	m^2	1.3e−14	

modelling in a 2D axisymmetric configuration. Due to the geometrical constraint of the semi-analytical solutions, horizontal well KB501 is simplified to a vertical well. We assume that this simplification is valid because the approximately 70-km^2 area influenced by the injection is large compared to the 2-m-long well.[5] In addition, because the aquifer is very thin (20 m in thickness), the injection-induced pressurization forms a bulb-like pressure zone that covers the entire well and extends in the radial direction, as observed in Rutqvist et al.[8]

As shown in Fig. 7, the model consists of a 900-m-thick surface layer, 900-m-thick impermeable caprock and a 20-m-thick aquifer where CO_2 is to be injected at a rate of approximately 8 kg/s. The material properties of the injection zone are presented in Table 2.

Fig. 8 compares the results of the semi-analytical solutions and the actual measurements for the three-year injection. Both semi-analytical solutions indicate an approximately 7-mm surface uplift after the first two years, consistent with the detected surface uplift, but underestimate the uplift in the third year. The computed results of Rutqvist et al.[8] are the same order of magnitude as the measurement in the third year, but the uplift during the first two years is underestimated. A bell-shaped uplift form is observed, as shown in Fig. 9. The spatial pattern of surface uplift is consistent with the uplift spread computed by

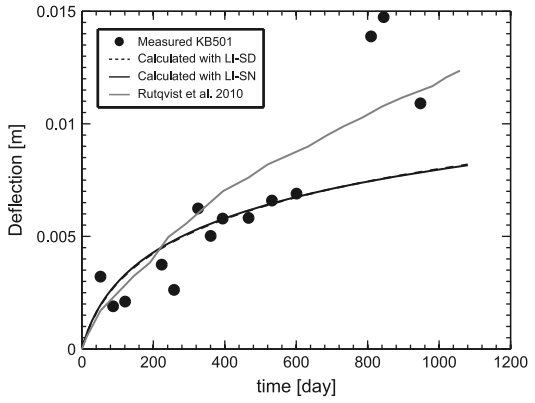

Fig. 8. Comparison of the calculated temporal surface uplift to the measured ground uplift over well KB501 and the numerical result calculated by Rutqvist et al.[8]

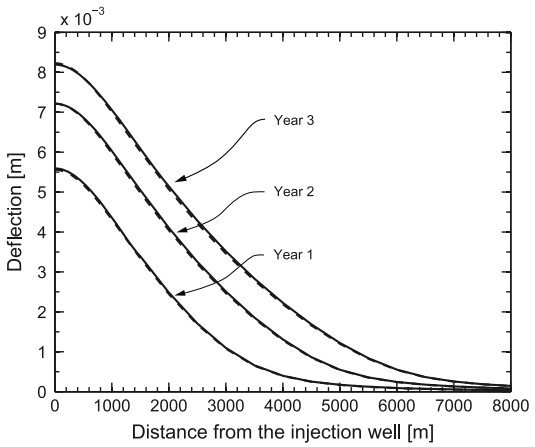

Fig. 9. Calculated surface uplift over well KB501.

Preisig and Prévost[7] and the satellite imagery presented in Onuma and Ohkawa[5] and Bohloli et al.[6]

7. Conclusion

The injection of CO_2 pressurizes the reservoir and causes caprock deflection, which further results in surface uplift. A semi-analytical approach was developed to predict the temporal and spatial deformation level of the caprock and the surface. The approach assumes linear elastic materials, the caprock as a thin-plate, an abrupt CO_2-water interface and no capillary forces. In developing the analytical model, we accounted for an arbitrary pressurization distribution within the injection zone, followed by a mathematical formulation of caprock deflection subjected to such pressure loading. Next, we incorporated two overpressure distribution functions to address the CO_2 injection-induced pressurization. After including the pressure-dependent CO_2 density and viscosity, the mathematical modelling led to two closed-form analytical expressions to address the mechanical interaction between the primary caprock and adjacent regions that is affected by the CO_2 injection-induced pressurization.

The developed solutions were applied to a representative CO_2 storage case that was solved numerically by the finite element method. The analytical results match the numerical simulation results, demonstrating the relevancy of the approximations and assumptions implemented in the development. Parametric studies were undertaken to illustrate the influence of factors such as geometry, overpressure magnitude and material properties on the caprock deflection. Finally, we benchmarked the developed semi-analytical solutions to assess the surface uplift observed at In Salah. Good agreement in the temporal and spatial evolution was observed between the measurements and the calculated results.

The advantage of using a semi-analytical approach is that it offers a convenient and efficient way to assess the impact of various factors and material parameters on the safety of CO_2 injection projects. In view of the computational approaches, the developed semi-analytical approach is an alternative and cost-effective calculation tool for preliminary candidate site evaluation and sensitivity analysis. In addition, the development within this paper is straightforward. Other fluid injection-induced pressurization distribution functions can be incorporated into the mechanical part. Thus, this model can integrate advances in hydrology research and be extended to any fluid injection problem.

Appendix A. Error estimation

We have seen in the first part of this work that it is common to approximate $\int_{d-t/2}^{d+t/2} e^{-kx}\mathrm{d}x$ by te^{-kd} because the hyperbolic sinus $sh(x) \approx x$ when x is sufficiently small. However, in our case, it leads to the approximation: $sh(kt/2) \approx kt/2$. k varies from 0 to infinity, and t is a constant. The approximation we performed previously must be verified.

All integrals composing the $u_z^{(s)p}$ term must be examined.

We have the following:

$$u_z^{(s)p}(r,0) = \frac{b}{G_s}\int_0^\infty\int_0^\infty p(\rho) \cdot g_z(r, z=0; \rho, d)\,\mathrm{d}\rho\mathrm{d}d \tag{A.1}$$

with:

$$g_z(r, z=0; \rho, d) = -(1-2\nu_s)\,\rho\int_0^\infty \xi J_0(\xi r)J_0 \times (\xi\rho)e^{-\xi d}\mathrm{d}\xi. \tag{A.2}$$

For simplification and without loss of generality, we assume that the pressure is constant over radius R from the injection well (otherwise we work with an inequality and the maximum pressure over the domain).

$$P(r,z) = \Delta PH(R-\rho) \quad \text{if } d-\frac{t}{2} \le z \le d+\frac{t}{2}$$
$$P(r,z) = 0 \quad \text{otherwise.} \tag{A.3}$$

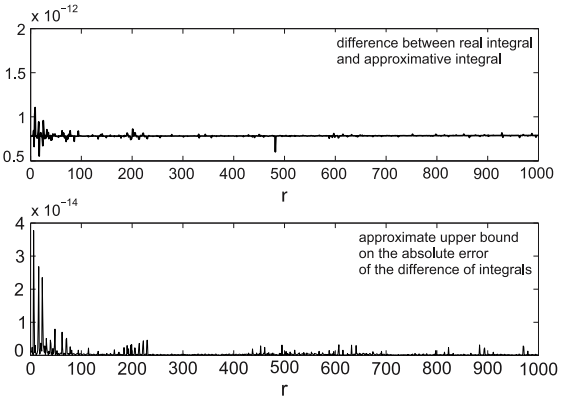

Fig. A.1. Error estimation of the approximation employed in the development.

This gives the following:

$$u_z^{(s)p}(r,0) = -\frac{(1-2\nu_s)\,b\Delta PR}{G_s}\int_0^\infty J_0(kr)\,J_1(kR) \times \frac{2}{k}e^{-kl}sh\left(\frac{kt}{2}\right)\mathrm{d}k \equiv u. \tag{A.4}$$

If we performed the previous approximation, we would have obtained the same result as Eq. (10) in[19]:

$$u_z^{(s)p}(r,0) = -\frac{(1-2\nu_s)\,b\Delta PR}{G_s}\int_0^\infty tJ_0(kr) \times J_1(kR)\,e^{-kl}\mathrm{d}k \equiv \tilde{u}. \tag{A.5}$$

Setting $C = -\frac{(1-2\nu_s)b\Delta PR}{G_s}$, we obtain the following:

$$\left(u-\tilde{u}\right)(r) = C\int_0^\infty\left(\frac{2}{k}sh\left(\frac{kt}{2}\right)-t\right) \times J_0(kr)\,J_1(kR)\,e^{-kl}\mathrm{d}k. \tag{A.6}$$

To study the problem, we examine the behaviour of the previous function as a function of r, throughout the numerical computation. For the best computation, we can change the variable:

$$\mathbb{R}^+ \to [0;1[$$
$$\varphi : y \to \mathrm{argth}(y) = \frac{1}{2}\ln\left(\frac{1-y}{1+y}\right). \tag{A.7}$$

This gives the following:

$$\left(u-\tilde{u}\right)(r) = -C\int_0^1\left(\left(\frac{2}{\mathrm{argth}(y)}sh\left(\frac{\mathrm{argth}(y)t}{2}\right)-t\right) \times J_0(\mathrm{argth}(y)r)\,J_1(\mathrm{argth}(y)R) \times e^{-\mathrm{argth}(y)l}\frac{y}{1-y^2}\right)\mathrm{d}y. \tag{A.8}$$

We observe that the difference is very small (approximately 10^{-13}) compared to the value of u or $\tilde{u}$ (approximately 10^{-3}–10^{-2}), as shown in Fig. A.1.

Appendix B. Finite element numerical model

A typical CO_2 storage model in an axisymmetric configuration is proposed to compare the numerical and analytical solutions. The model, which consists of 9273 4-node quadrilateral elements, is shown in Fig. B.1. The model includes an 800-m-thick overburden layer, a 100-m-thick caprock layer and a 100-m-thick aquifer into which CO_2 is injected at a constant flow rate through a vertical well. The model is 10 km in size to simulate the infinite-acting aquifer of the analytical solution. On the outer boundary of the model, a hydrostatic pressure is applied, and displacements are fixed.

The materials involved in the problem are porous media, which are treated as a mixture consisting of a solid matrix, water and CO_2 phases according to the theory of mixtures[29] which is implemented by Collin et al.[27] in the nonlinear finite element code Lagamine.[30] The code is used to solve the mass conservation equations for water, w, and CO_2, c and the momentum equation. In the following, a brief summary of the coupled system is introduced to solve for the displacement of solid matrix $\boldsymbol{u}$, water pressure p_w and CO_2 pressure p_c.

The mass conservation equations are written for water and CO_2:

$$\frac{\partial\left(nS_\alpha\rho_\alpha\right)}{\partial t} + \mathbf{div}\left(\rho_\alpha\mathbf{f}_\alpha\right) = 0; \quad \alpha = c, w \tag{B.1}$$

where n is the porosity, S_α is the degree of saturation of the α-phase, ρ_α is the density and $\mathbf{f}_\alpha$ is the velocity of the α-fluid, which is defined by the generalized Darcy's law for porous media:

$$\mathbf{f}_\alpha = \frac{k_{\mathrm{int}}k_{r,\alpha}}{\mu_\alpha}\left(\mathbf{grad}\left(p_\alpha\right) + \rho_\alpha g\,\mathbf{grad}\left(z\right)\right) \tag{B.2}$$

in which μ_α is the dynamic viscosity of α phase, k_{int} is the intrinsic permeability of the reservoir rock, $k_{r,\alpha}$ is the relative permeability of the α-fluid and p_α is the α fluid pressure.

A van Genuchten function[26] is used to describe the retention behaviour of the reservoir rock:

$$S_w = \left(1+\left(s/P_0\right)^{1/(1-\lambda)}\right)^{-\lambda} \tag{B.3}$$

where λ and P_0 are a material parameter and a reference pressure, respectively, and s is the matrix suction or capillary pressure defined as the difference between CO_2 and water pressure, $s = p_c - p_w$. A linear function for relative permeability is used:

$$k_\alpha = S_\alpha. \tag{B.4}$$

The momentum equation is written as follows:

$$\mathrm{div}\left(\boldsymbol{\sigma}\right) + \rho\mathbf{g} = 0 \tag{B.5}$$

where ρ is the density of the mixture, which is defined as follows:

$$\rho = (1-n)\,\rho_s + nS_w\rho_w + n\left(1-S_w\right)\rho_c \tag{B.6}$$

and the total stress $\boldsymbol{\sigma}$ can be decomposed through a combination of the generalized effective stress tensor $\boldsymbol{\sigma}'$, water pressure p_w and CO_2 pressure p_c:

$$\boldsymbol{\sigma}' = \boldsymbol{\sigma} - p_c\mathbf{I} + S_w\left(p_c - p_w\right)\mathbf{I}. \tag{B.7}$$

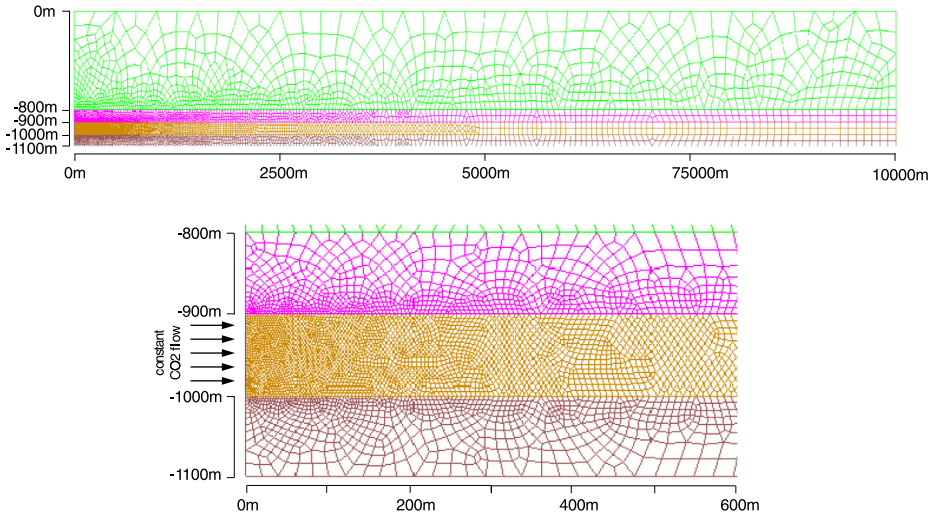

Fig. B.1. Numerical model mesh used for simulation. Details in the vicinity of the well are magnified.

All materials are considered linear elastic. The stress–strain relationship is described below:

$$d\boldsymbol{\varepsilon} = \mathbf{E}^{-1} d\boldsymbol{\sigma}' \tag{B.8}$$

where $\mathbf{E}$ is the elastic tensor and $d\boldsymbol{\varepsilon}$ is the strain tensor increment, and the strain is defined as $\boldsymbol{\varepsilon} = 1/2\left(\nabla \mathbf{u} + \nabla^{\mathrm{T}} \mathbf{u}\right)$.

References

[1] Reichle D, Houghton J, Kane B, Ekmann J. Carbon sequestration research and development, December 1999.

[2] Bryant E. *Climate Process and Change*. Cambridge, UK: Cambridge University Press; 1997.

[3] Bachu S. Sequestration of CO_2 in geological media: criteria and approach for site selection in response to climate change. *Energy Convers. Manage.* 2000;41(9):953–970.

[4] Ringrose PS, Mathieson AS, Wright IW, Selama F, Hansen O, Bissell R, Saoula N, Midgley J. The In Salah CO_2 storage project: Lessons learned and knowledge transfer. *Energy Procedia*. 2013;37:6226–6236.

[5] Onuma T, Ohkawa S. Detection of surface deformation related with CO_2 injection by DInSAR at In Salah, Algeria. *Energy Procedia*. 2009;1(1):2177–2184.

[6] Vasco DW, Ferretti A, Novali F. Reservoir monitoring and characterization using satellite geodetic data: Interferometric synthetic aperture radar observations from the Krechba field, Algeria. *Geophysics*. 2008;73(6):WA113–WA122.

[7] Preisig M, Prévost JH. Coupled multi-phase thermo-poromechanical effects. Case study: CO_2 injection at In Salah, Algeria. *Int. J. Greenhouse Gas Control*. 2011;5(4):1055–1064.

[8] Rutqvist J, Vasco DW, Myer L. Coupled reservoir-geomechanical analysis of CO_2 injection and ground deformations at In Salah, Algeria. *Int. J. Greenhouse Gas Control*. 2010;4(2):225–230.

[9] Rohmer J, Seyedi DM. Coupled large scale hydromechanical modelling for Caprock failure risk assessment of CO_2 Storage in Deep Saline Aquifers. *Oil Gas Sci Technol. Rev. Inst. Fr. Pét.* 2010;65(3):503–517.

[10] Vilarrasa V, Bolster D, Olivella S, Carrera J. Coupled hydromechanical modeling of CO_2 sequestration in deep saline aquifers. *Int. J. Greenhouse Gas Control*. 2010;4(6):910–919.

[11] Rutqvist J. The geomechanics of CO_2 storage in deep sedimentary formations. *Geotech. Geol. Eng.* 2012;30(3):525–551.

[12] Fjar E, Holt RM, Raaen AM, Risnes R, Horsrud P. *Petroleum Related Rock Mechanics. Vol. 2008*. 2nd ed. 2008.

[13] Geertsma J. Land subsidence above compacting oil and gas reservoirs. *J. Pet. Technol.* 1973;25(06):734–744.

[14] Selvadurai APS. Mechanics of an embedded caprock layer during pressurization of a CO_2 storage reservoir. In: *Proceedings of ComGeo 09: Computational Geomechanics I*, 2008: 466–475.

[15] Selvadurai APS. Heave of a surficial rock layer due to pressures generated by injected fluids. *Geophys. Res. Lett.* 2009;36(14):L14302.

[16] Nordbotten JM, Celia MA, Bachu S. Injection and storage of CO_2 in deep saline aquifers: Analytical solution for CO_2 plume evolution during injection. *Transp. Porous Media*. 2005;58(3):339–360.

[17] Dentz M, Tartakovsky DM. Abrupt-interface solution for carbon dioxide injection into porous media. *Transp. Porous Media*. 2008;79(1):15–27.

[18] Selvadurai APS. *Partial Differential Equations in Mechanics 2: The Biharmonic Equation, Poisson's Equation*. Springer; 2000.

[19] Segall P, Grasso J-R, Mossop A. Poroelastic stressing and induced seismicity near the Lacq gas field, southwestern France. *J. Geophys. Res.* 1994;99(B8):15423.

[20] Bear J. *Dynamics of Fluids in Porous Media*. 1972.

[21] Lu C, Lee S-Y, Han WS, McPherson BJ, Lichtner PC. Comments on "Abrupt-interface solution for carbon dioxide injection into porous media" by M. Dentz and D. Tartakovsky. *Transp. Porous Media*. 2009;79(1):29–37.

[22] Dentz M, Tartakovsky DM. Response to "Comments on abrupt-interface solution for carbon dioxide injection into porous media by Dentz and Tartakovsky (2008)" by Lu et al. *Transp. Porous Media*. 2009;79(1):39–41.

[23] Vilarrasa V, Bolster D, Dentz M, Olivella S, Carrera J. Effects of CO_2 compressibility on CO_2 storage in deep saline aquifers. *Transp. Porous Media*. 2010;85(2):619–639.

[24] Peng D-Y, Robinson DB. A new two-constant equation of state. *Ind. Eng. Chem. Fundam.* 1976;15(1):59–64.

[25] Fenghour A, Wakeham WA, Vesovic V. The viscosity of carbon dioxide. *J. Phys. Chem. Ref. Data*. 1998;27(1):31.

[26] van Genuchten MT. A closed-form equation for predicting the hydraulic conductivity of unsaturated soils1. *Soil Sci. Soc. Am. J.* 1980;44(5):892.

[27] Collin F. *Couplages Thermo-Hydro-Mécaniques dans les sols et les Roches Tendres Partiellement Saturés*. Belgium: University of Liège; 2003.

[28] Bohloli B, Aker E, Cuisiat F, Oye V, Khn D. Analysis of pressure versus flow regime of CO_2 To assess matrix and fracture injection at In Salah, Algeria. In: *Third EAGE* CO_2 *Geological Storage Workshop*, March 2012; 2012: 26–28.

[29] Bowen RM. Compressible porous media models by use of the theory of mixtures. *Internat. J. Engrg. Sci.* 1982;20(6):697–735.

[30] Charlier R, Radu J-P, Collin F. Numerical modelling of coupled transient phenomena. *Rev. Française Génie Civ.* 2011.